Article:
Li, W, Shi, Y, Hu, X et al. (6 more authors) (2019) Visual detection of nitrite in sausage based on a ratiometric fluorescent system. Food Control, 106. 106704. ISSN 0956-7135

https://doi.org/10.1016/j.foodcont.2019.06.030

Visual detection of nitrite in sausage based on a ratiometric fluorescent system

Wenting Li [a, &], Yongqiang Shi [a, &], Xuetao Hu [a, &], Zhihua Li [a], Xiaowei Huang [a], Melvin Holmes [b, c], Yunyun Gong [b, c], Jiyong Shi [a, c, *], Xiaobo Zou [a, c, *]

a Agricultural Product Processing and Storage Lab, School of Food and Biological Engineering, Jiangsu University, Zhenjiang, Jiangsu 212013, China

b School of Food Science and Nutrition, University of Leeds, Leeds LS2 9JT, United Kingdom

c China-UK joint laboratory for nondestructive detection of agro-products, Jiangsu University, Zhenjiang, Jiangsu 212013, China

& Contributed equally to this work

*Corresponding author:

Prof. Jiyong Shi

School of Food and Biological Engineering,

Jiangsu University, Zhenjiang 212013, China.

E-mail: Shi_jiyong@ujs.edu.cn.

Prof. Xiaobo Zou

School of Food and Biological Engineering,

Jiangsu University, Zhenjiang 212013, China.

E-mail: zou_xiaobo@ujs.edu.cn.

Tel.:+86-0511-88790958

Abstract

A novel ratiometric fluorescence sensor based on fluorescence resonance energy transfer (FRET) between MoS_2 QDs and AuNCs was developed for nitrite detection in sausages. The MoS_2 QDs-AuNCs nanocomposite exhibited dual emission peaks at 430 nm and 615 nm under 365 nm excitation. With addition of nitrite, the fluorescence of AuNCs was quenched due to the agglomeration of AuNCs, whereas the emission of MoS_2 QDs increased for the blocked FRET. With this strategy, nitrite was detected in the range of 0.5 – 20 mg/L with a detection limit of 0.67 nM. Furthermore, based on the fluorescence color change of the sensor at different nitrite concentration, a microfluidic chip combined with smartphone was developed for the fluorescent visual detection of nitrite over a range of 1.0 – 20 mg/L. Finally, the developed methods were applied to the determination of nitrite in sausage samples with the satisfactory recoveries of 102.6%-110.8%, indicating the potential for practical application.

Keywords: MoS_2 QDs; AuNCs; Nitrite; Ratiometric fluorescence; Fluorescence visualization

1 Introduction

Chinese sausage is a popular meat product in China due to its specific flavors and taste. Nitrite, as a permitted food additive, is often used in sausage for inhibiting the growth of microorganisms and improving the color and flavor (Iacumin, et al., 2019). However, excessive presence of nitrite will cause serious health hazard to the public such as methemoglobinemia, occasional intoxications and potential cancer (Ding, Gao, & Li, 2018; Viboonratanasri, Pabchanda, & Prompinit, 2018). Therefore, rapid and accurate detection of nitrite content in sausage is of great importance for food safety control and regulation.

Conventional detection methods for nitrite including high-performance liquid chromatography (H. Li, Meininger, & Wu, 2000), spectroscopy (Zheng, Liang, Li, Zhang, & Qiu, 2016), chromatography (Niedzielski, Kurzyca, & Siepak, 2006), capillary electrophoresis (Ruri Kikurahanajiri, And, & §, 2002) and electrochemical methods (Wan, Zheng, Wan, Yin, & Song, 2017). Although these techniques are stable and reliable, most of them require expensive instrumentation and complicated operations (Gu, et al., 2016). In comparison, fluorescence analysis may be an ideal selection for nitrite detection owing to its easy operation, high sensitivity and low-cost (Hu, Shi, Shi, Zou, Arslan, et al., 2019; Y. Xu, et al., 2015).

Fluorescence probes for nitrite detection have been reported previously (Hu, Shi, Shi, Zou, Tahir, et al., 2019; Qi, You, & Chen, 2016; Q. Wang, et al., 2016). For instance, A 2-(1H-phenanthro[9、10-d] imidazol-2-yl)aniline (PA) fluorescence probe was developed for nitrite detection in sausage based on a novel NO_2^--mediated diazozation and subsequent cyclization (Gu, et al., 2016). Wang et al. (Q. Wang, et al., 2016) used the reaction of nitric oxide with a dihydropyridine derivative to form a highly fluorescent pyridine derivative achieving ultralow detection limit of 0.02 μmol/L. However, most of the above fluorescence probes used a single fluorescence peak as response signal, which may be susceptible to the probe concentration, fluctuation of excitation intensity and environmental interference (Santoro, et al., 2016). By contrast, ratiometric fluorescence (RF) probes, based on the ratio of the dual fluorescence peaks,

could greatly reduce interference and improve the sensitivity for target analytes (Kaur, et al., 2018). Fluorescence resonance energy transfer (FRET) has been the most commonly applied mechanism for RF probe development due to the superiority of design flexibility and reduction of auto-fluorescence (Xue, Wang, Ouyang, & Qiu, 2019). Various FRET-based RF probes have been employed for analyte sensing such as hypochlorous acid (Shen, et al., 2018), cysteine (Yu, et al., 2018) and protein (H. Li, Zhao, Chen, & Xu, 2017), which indicates FRET-based RF probes have great application prospects. However, to our knowledge, there are few reports on nitrite detection based on this strategy.

Previous study suggested that Molybdenum disulfide quantum dots (MoS_2 QDs) strongly emit in blue wavelength under UV excitation owing to the transition from the K point of Brillouin zone (Ha, Han, Choi, Park, & Seo, 2014), which makes MoS_2 QDs an ideal donor for FRET. Besides, gold nanoclusters (AuNCs) have great potential for the construction of dual-emission nanocomposites owing to their strong fluorescence intensity, large Stokes-shift and biocompatibility (X. Yang, et al., 2016). Therefore, it might be a promising method to develop a RF probe for nitrite detection by combining MoS_2 QDs and AuNCs. Moreover, Microfluidic analysis system, as a powerful analytical tool, have been widely used for nitrite detection (Ortiz-Gomez, et al., 2016) (Bhakta, Borba, Taba, Garcia, & Carrilho, 2014) (Beaton, et al., 2011). Combining microfluidic chip with MoS_2 QDs-AuNCs fluorescence probe might greatly improve the detection performance for nitrite.

Herein, a novel FRET-based RF sensor and a fluorescence colorimetric microfluidic chip were developed for the nitrite detection. Under 365 nm excitation, the emission of BSA–AuNCs could be quenched by nitrite, resulting in the fluorescence recovery of MoS_2 QDs. According to the phenomenon, nitrite was quantified based on the ratio of fluorescence intensities at two wavelengths, and the detection mechanisms were discussed in detail. Furthermore, according to the changes of fluorescence color with the increase of nitrite concentration, a microfluidic chip combined with a smart phone was designed and used to achieve the fluorescence visual detection of nitrite.

Finally, the proposed fluorescence and visualization methods were successfully applied to nitrite detection in sausage.

2 Materials and methods

2.1 Reagents and apparatus

Glutathione (GSH), Sodium molybdate ($Na_2MoO_4 \cdot 2H_2O$), 1-ethyl-3-(3-(dimethylamino)propyl)-carbodii-mide (EDC) and N-hydroxy-sulfosuccinimide (NHS) were obtained from Sigma-Aldrich (Shanghai, China). The remaining reagents (e.g., $HAuCl_4 \cdot 4H_2O$, bovine serum albumin (BSA) and sodium nitrite) were purchased from Sinopharm Chemical Reagent Co., Ltd (Shanghai, China). All the reagents used were of analytical grade. Deionized water (18 MΩ/cm) was used in all experiments.

The fluorescence was measured using F98 fluorescence spectrometer (Lengguang technology, Shanghai, China). The morphology and structure of MoS_2-AuNCs were characterized using JEM-2000 high resolution transmission electron microscopy (HRTEM) (JEOL, Tokyo, Japan). The UV–vis absorption spectra were recorded on a UV-1601 spectrometer (Beifen-Ruili, Beijing, China). FT-IR spectra were performed on a Nicolet IS50 FT-IR spectrometer (Thermo Scientific, Massachusetts, USA). The X-ray diffraction (XRD) spectrum were obtained from a D8 Advance diffractometer (Bruker, Karlsruhe, Germany). The fluorescent lifetime spectrum was measured by QuantaMaster™ 40 Fluorescence Lifetime Spectrometers (PTI, USA).

2.2 Synthesis and preparation of materials

2.2.1 Synthesis of MoS_2 QDs

The MoS_2 QDs were synthetized through a hydrothermal method (Swaminathan & Balasubramanian, 2018). Briefly, 0.25 g $Na_2MoO_4 \cdot 2H_2O$ was dissolved in 20 mL of deionized water followed by sonication for 10 min. Then the solution was adjusted to pH 6.5 by 0.1 M of HCl. 0.5 g of GSH was subsequently added to the solution and sonicated for 10 min again. The resulting mixture was transferred to Teflon-lined stainless steel autoclave and reacted at 200 °C for 24 h. Finally, when the solution cooled naturally, the supernatant was collected after centrifugation at 12000 rpm for

30 min.

2.2.2 Preparation of AuNCs

The BSA-stabilized AuNCs were prepared according to the reported methods (Xu, Qiao, Li, Qi, & Zhang, 2015) with some modification. 5.0 mL of BSA solution (50.0 mg/mL) was mixed with 5.0 mL of $HAuCl_4$ solution (10.0 mM) under magnetic stirring for 2 min. Then 0.5 mL of NaOH solution (1.0 mM) was added to adjust to pH 12. After that, the mixture was sonicated for 4 h at room temperature. The resultant brown AuNCs was purified via dialysis membrane (1000 Da) and stored at 4 °C for further use.

2.2.3 Preparation of MoS_2 QDs-AuNCs nanohybrid.

The MoS_2 QDs-AuNCs nanohybrid was prepared via coupling reaction using EDC/NHS technique (Niu, et al., 2016). Specifically, 500 μL of EDC/NHS aqueous solution (10 mg/mL for each) was added to 6 mL of AuNCs solution followed by stirring for 30 min at 4 °C to activate the carboxyl group. Then 10 mL of prepared MoS_2 QDs solution was added and the mixture was incubated under vigorous stirring for 12 h.

2.3 Ratiometric fluorescence detection of nitrite

Firstly, 1.0 mL of MoS_2 QDs-AuNCs solution was mixed with different amount of $NaNO_2$ followed by dilution to 5 mL with PBS solution. The final concentration of $NaNO_2$ were 0, 0.1, 0.5, 1, 2, 5, 8, 10, 15, 20, 25, 30, 40 and 50 mg/L, respectively. Then the mixture was incubated for 7 min under ambient temperature. The fluorescence spectrum of MoS_2 QDs-AuNCs nanohybrid was recorded upon excitation at 365 nm. All measurements were performed three times at room temperature.

2.4 Fluorescence visualization analysis for nitrite

A quantitative model was established on the dependence of fluorescence color on nitrite concentrations. Firstly, Fluorescence color of the MoS_2 QDs-AuNCs system was collected employing the microfluidic chips and image acquisition device (seen in the supplementary materials), and the results showed fluorescence color of the probe changed from red to blue with increase in nitrite concentration. Then the images obtained were processed through OpenCV image library based on Android platform.

Specifically, background region and reaction cell were firstly segmented with the powerful function of OpenCV. Because the single channel color information in RGB mode can not accurately describe fluorescence color change of the system, the segmented RGB images were then transformed into L*a*b model images. Next, the channel "a" images were separated from L*a*b images, and average "a" values were calculated according to gray information of the pixels. Finally, Standard curve was established on the dependence of "a" values on nitrite concentrations.

2.5 Nitrite detection in sausage samples

Firstly, sausage samples (Shuanghui food Co., Luohe, China) were purchased from nearby supermarket. Then they were pretreated according to the reported literature (B.-L. Li, Li, & Gao, 2019). Finally, nitrite contents in the sausages were determined based on the methods described in "Ratiometric fluorescence detection of nitrite" and "Fluorescence visualization analysis for nitrite".

3 Results and discussion

3.1 Characterizations of prepared materials

The morphology and dimensions of prepared materials were investigated by HRTEM. Fig.1 A displays the TEM images of as-synthesized MoS_2 QDs. It can be found the compounds are uniformly dispersed with the size ranging from 4 to 8 nm. The lattice of 0.21 nm shown in the inset corresponds to the Mo (110), which is consistent with previous report (Duan, et al., 2018). Fig.1 B illustrates that the particle size distribution of BSA-AuNCs ranges from 3 to 5 nm with the lattice of 0.25 nm (Sun, Yang, Zhao, & Yang, 2014). Compared with the single MoS_2 QDs or AuNCs, MoS_2 QDs-AuNCs composite shown in Fig.1 C has larger size, and the different lattice spacing indicates the successful preparation of the MoS_2 QDs-AuNCs composite.

Fig.1

The crystal structures of MoS_2 QDs-AuNCs composite were further explored by X-ray diffraction (XRD). As shown in Fig.1 D, the diffraction peaks at $2\theta = 14°$, 33°,

40° and 59° are ascribed separately to the (002), (100), (103) and (110) planes of hexagonal phase MoS_2 while the peaks at higher 2θ angles are indexed to the (111), (200), (220), and (311) planes of face-centered cubic Au (J. Yang, Elim, Zhang, Lee, & Ji, 2006; Ze, Yueqiu, Xujun, & Yong, 2017). The results indicate that the MoS_2 QDs-AuNCs composite has signals of both MoS_2 QDs and AuNCs.

The surface composition of the obtained MoS_2 QDs-AuNCs composite was investigated by FT-IR spectra. As shown in Fig.1 E, AuNCs have the characteristic peaks associated with BSA at ~3277, 1654, 1457 and 1351 cm^{-1}, which are attributed to O—H stretching, C═O stretching, N—H stretching and C—N stretching vibrations, respectively. Notably, the disappearance of S—H characteristic peaks at ~2525 cm^{-1} indicated that the thiol groups of BSA acted as reductant in the synthesis of AuNCs (Xie, et al., 2018). As for the MoS_2 QDs, apart from the characteristic peaks similar to the AuNCs, the other observed peaks around 3255, 2924, 1064 and 885 cm^{-1} are assigned to —NH_2, C—H, C—O and C—O—C stretching vibration mode, respectively. The above results confirmed that the surfaces of MoS_2 QDs and AuNCs were modified with active groups. For the MoS_2 QDs-AuNCs composite, the peak intensity of band in 1200−1650 cm^{-1} decreased obviously compared with that of the prepared MoS_2 QDs, which indicates the interaction between MoS_2 QDs and AuNCs.

The UV–vis absorption spectrums of the MoS_2 QDs and AuNCs were shown in Fig.1 F. A distinct absorption peak centered near 340 nm could be found in the spectrum of AuNCs, which was assigned to n − π* transitions of C═O groups (Xie, et al., 2018). More importantly, there is a broad absorption at 370–450 nm, which provides conditions for the construction of fluorescence resonance energy transfer (FRET) system. The absorption spectrum of the prepared MoS_2 QDs showed no absorption peak from 500 to 600 nm, this characteristic agrees with the result reported before (Lin, et al., 2019).

3.2 FRET behavior between MoS_2 QDs and AuNCs

A ratiometric fluorescence nanoprobe was developed based on FRET strategy. Fig.2 A shows the fluorescence emission spectrums of the prepared composites under

365 nm excitation. The peaks centered at 430 and 615 nm respectively correspond to the PL emission of MoS_2 QDs and AuNCs. Furthermore, the quantum yields (QY) determined for the MoS_2 QDs and AuNCs were 13.4% and 19.6% with quinine sulfate as the standard. The MoS_2 QDs-AuNCs nanocomposite displayed dual emission peaks at 430 and 615 nm. Remarkably, the emission intensity of MoS_2 QDs decreased significantly. Then the effect of AuNCs on fluorescence performance of MoS_2 QDs was explored at 365 nm excitation. As shown in Fig.2 B, the FL intensity of MoS_2 QDs decreased gradually with the addition of AuNCs from 0 to 600 μL, which may be attributed to the occurrence of FRET.

Fig.2

To prove this conjecture, fluorescence and absorption spectrums of MoS_2 QDs and AuNCs were studied. The efficiency of FRET is dependent upon donor-acceptor proximity (<10 nm) and spectral overlap. As shown in Fig.2 C, the absorption spectra of AuNCs overlapped with the fluorescence emission spectra of MoS_2 QDs from 390 nm to 550 nm. On the other hand, according to the TEM image in Fig.1 C, the distance between MoS_2 QDs and AuNCs was less than 10 nm due to the coupling between two fluorofores. The results above confirmed the occurrence of FRET between MoS_2 QDs and AuNCs. Then the fluorescence lifetime of MoS_2 QDs and MoS_2 QDs-AuNCs composites were measured to study the quenching mechanism. As shown in Fig.2 D, the introduction of AuNCs reduced fluorescence lifetime of MoS_2 QDs from 6.97 ns to 2.45 ns, indicating the fluorescence quenching of MoS_2 QDs by AuNCs was dynamic quenching.

3.3 Effect of nitrite on fluorescence of MoS_2 QDs-AuNCs composite

The effect of nitrite on fluorescence of MoS_2 QDs-AuNCs composite and possible sensing mechanism were studied. As shown in Fig.3, under 365 nm excitation, the fluorescence intensity of MoS_2 QDs at 430 nm remained nearly unchanged with the presence or absence of 10 mg/L nitrite. However, the addition of same amount of nitrite induced fluorescence quenching of AuNCs at 615 nm. The quenching mechanism could

be attributed to the aggregation of AuNCs caused by the interaction between NO_2^- and BSA ligands coated on the surface of AuNCs, and an effective charge transfer from Au to NO_2^- was built instead of that of BSA-to-Au, leading to the fluorescence quenching of AuNCs (Liu, Yang, Abdel-Halim, & Zhu, 2013; L. Wang, et al., 2019). For the MoS_2 QDs-AuNCs system, the fluorescence of AuNCs quenched while that of MoS_2 QDs recovered after adding 10 mg/L of NO_2^- to the system, which may be ascribed to the blocked FRET process resulting from the aggregation of AuNCs. Thus, the detection of nitrite was achieved according to the changes in I_{615}/I_{430} (I_{615} and I_{430} represent the fluorescence intensity at 615 nm and 430 nm). From the above discussion, the schematic diagram for detecting nitrite by employing the proposed MoS_2 QDs-AuNCs system was shown in Fig.4.

Fig.3

Fig.4

3.4 Optimization of the experimental conditions

The pH and reaction time were optimized for MoS_2 QDs-AuNCs probe. As shown in Fig.5 A, I_{615}/I_{430} increased with the pH from acidity to weak alkalinity but decreased at strong alkaline condition. This phenomenon may be due to the fact that strong acid or alkali media changed the secondary structure of ligand BSA, which plays a key role in the fluorescence properties of AuNCs (Cao, et al., 2015). Accordingly, weak alkali media of pH 8.5 was optimal for the fluorescent probe. Fig.5 B displayed the effect of reaction time on response of the sensing system exposed to nitrite of 10 mg/L. It can be found the response value (I_{615}/I_{430}) tended to be stable after reaction time of 7 minutes, indicating the reaction has been completed. Therefore, reaction time of 7 minutes was selected for the further experiments.

Fig.5

3.5 Ratiometric fluorescence detection of nitrite

The fluorescence responses of the MoS_2 QDs-AuNCs system in the presence of different concentrations of nitrite were measured under the optimized condition. As shown in Fig.6 A, with increase in nitrite concentration, the fluorescence signal of AuNCs at 615 nm was quenched by nitrite while that of MoS_2 QDs at 430 nm was enhanced. Fig.6 B displayed that the fluorescence intensity ratio of the AuNCs and MoS_2 QDs (I_{615}/I_{430}) decreased gradually with the concentration of nitrite increased from 0-50 mg/L. From the insert of Fig.6 B, a linear calibration can be found in the concentration range of 0.5-20 mg/L with a regression equation of I_{615}/I_{430} = -0.084C+2.693 (C is the concentration of nitrite in mg/L, R^2=0.991). The detection limit for nitrite calculated according to 3σ/s was 0.67 nM, where σ represents the standard deviation of eight blank measurements, and s is the slope of the calibration curve. More importantly, the fluorescence color change could be observed with increase in nitrite concentration from the insert of Fig.6 A, which renders visual detection of nitrite possible.

Fig.6

3.6 Sensing selectivity

To investigate the selectivity of the proposed methods, various interfering substances (including K^+, Cl^-, SO_3^{2-}, Glu, Ca^{2+}, Mg^{2+}, $H_2PO_4^-$, Fe^{3+}, CO_3^{2-}, NO_3^-) were selected to study their effects on the fluorescence responses of the MoS_2 QDs-AuNCs probe. The concentration of nitrite is 10 mg/L while other analytes are fixed at 20 mg/L. Fig.S2 reveals that I_{615}/I_{430} changed obviously in the presence of NO_2^- while no significant response changes were observed for the interfering substances compared with the blank control, which may be attributed to the specific interaction between BSA-AuNCs and NO_2^-. Furthermore, the fluorescence colors of the identical interferences were checked in the same experimental condition. The insert in Fig.S2 showed that the interferences have little effect on the fluorescence color of the constructed system, indicating adequate specificity of the proposed method for nitrite.

3.7 Fluorescence visualization analysis for nitrite

A visualized detection method for nitrite was developed by combining a smart phone with microfluidic chip based on MoS_2 QDs-AuNCs probe. Detailed experimental scheme was depicted in the supplementary materials. The fluorescence color changes from red to blue can be found with increase in nitrite concentration (Fig.7 A). Then the obtained images of "a" channels were extracted from L*a*b mode by image processing functions (Fig.7 B), it is clear that the gray value of "a" channel decreased gradually with increase in nitrite concentration. As shown in Fig.7 C, the average "a" value exhibited a linear response to the nitrite concentration in the range of 1.0-20 mg/L. the regression equation can be express as $y=-1.045x+25.173$ ($R^2=0.994$), and the detection limit for nitrite is 27.32 nM. The sensing performances of prepared MoS_2 QDs-AuNCs system were compared with several previous reports. As shown in Table.1, the performance parameters of MoS_2 QDs-AuNCs system are comparable or better than those of reported probes. The above results reveal potential of the prepared MoS_2 QDs-AuNCs system for nitrite detection.

Fig.7

Table.1

3.8 Nitrite detection in sausage samples

In order to evaluate the practicability of the established methods, the ratiometric MoS_2 QDs-AuNCs probe and prepared microfluidic chip were applied to detect nitrite in sausage. Different amounts of nitrite standard solution (0.0, 5.0, 10.0, 15.0 mg/L) were spiked to the pretreated sample solutions before determination. The results are shown in Table.2. It is observed that the recoveries of the spiked samples for fluorescence method varied from 102.6% to 108.2% and for visualized analysis ranged from 104.6% to 110.8%, and the relative standard deviations (RSD) were below 2.6 %, indicating that the proposed methods can be applied to practical detection of nitrite in sausage samples.

Table.2

4 Conclusion

In summary, a ratiometric fluorescence probe based on FRET between MoS_2 QDs and AuNCs was developed for nitrite detection in sausage. With the addition of nitrite, the fluorescence of AuNCs was quenched, and further caused the fluorescence recovery of MoS_2 QDs due to the blocked FRET. With this strategy, nitrite could be detected with high sensitivity, good selectivity and low detection limit. Furthermore, according to the color changes of the fluorescence probe, a microfluidic chip was employed to achieve visualized detection of nitrite over a range from 1.0 to 20 mg/L. Finally, the proposed fluorescent and visualized methods were successfully applied to the determination of nitrite in sausage samples, indicating the potential for practical application.

Acknowledgement

The authors gratefully acknowledge the financial support provided by the National Key R&D Program of China (2018YFD0400800, 2017YFC1600805), the national natural science foundation of China (31601543, 31801631), and the Natural Science Foundation of Jiangsu Province (BK20180865).

References

Abbas, M. N., & Mostafa, G. A. (2000). Determination of traces of nitrite and nitrate in water by solid phase spectrophotometry. *Analytica Chimica Acta, 410*(1), 185-192.

Beaton, A. D., Sieben, V. J., Floquet, C. F. A., Waugh, E. M., Abi Kaed Bey, S., Ogilvie, I. R. G., Mowlem, M. C., & Morgan, H. (2011). An automated microfluidic colourimetric sensor applied in situ to determine nitrite concentration. *Sensors and Actuators B: Chemical, 156*(2), 1009-1014.

Bhakta, S. A., Borba, R., Taba, M., Garcia, C. D., & Carrilho, E. (2014). Determination of nitrite in saliva using microfluidic paper-based analytical devices. *Analytica Chimica Acta, 809*, 117-122.

Cao, X., Li, H., Lian, L., Xu, N., Lou, D., & Wu, Y. (2015). A dual-responsive fluorescence method for the detection of clenbuterol based on BSA-protected gold nanoclusters. *Analytica Chimica Acta, 871*, 43-50.

Ding, Y., Gao, Y., & Li, Z. (2018). Carbon quantum dots (CQDs) and Co(dmgH)2PyCl synergistically promote photocatalytic hydrogen evolution over hexagonal ZnIn2S4. *Applied Surface Science, 462*, 255-262.

Duan, F., Zhang, S., Yang, L., Zhang, Z., He, L., & Wang, M. (2018). Bifunctional aptasensor based on novel two-dimensional nanocomposite of MoS2 quantum dots and g-C3N4 nanosheets decorated with chitosan-stabilized Au nanoparticles for selectively detecting prostate specific antigen. *Analytica Chimica Acta, 1036*, 121-132.

Gu, B., Huang, L., Hu, J., Liu, J., Su, W., Duan, X., Li, H., & Yao, S. (2016). Highly selective and sensitive fluorescent probe for the detection of nitrite. *Talanta, 152*, 155-161.

Ha, H. D., Han, D. J., Choi, J. S., Park, M., & Seo, T. S. (2014). Photoluminescence: Dual Role of Blue Luminescent MoS2 Quantum Dots in Fluorescence Resonance Energy Transfer Phenomenon (Small 19/2014). *Small, 10*(19), 3858-3862.

Hu, X., Shi, J., Shi, Y., Zou, X., Arslan, M., Zhang, W., Huang, X., Li, Z., & Xu, Y. (2019). Use of a smartphone for visual detection of melamine in milk based on Au@Carbon quantum dots nanocomposites. *Food Chemistry, 272*, 58-65.

Hu, X., Shi, J., Shi, Y., Zou, X., Tahir, H. E., Holmes, M., Zhang, W., Huang, X., Li, Z., & Xu, Y. (2019). A dual-mode sensor for colorimetric and fluorescent detection of nitrite in hams based on carbon dots-neutral red system. *Meat Science, 147*, 127-134.

Iacumin, L., Cattaneo, P., Zuccolo, C., Galanetto, S., Acquafredda, A., & Comi, G. (2019). Natural levels of nitrites and nitrates in San Daniele dry cured ham PDO, and in meat, salt and sugna used for its production. *Food Control, 100*, 257-261.

Kaur, N., Kaur, M., Chopra, S., Singh, J., Kuwar, A., & Singh, N. (2018). Fe(III) conjugated fluorescent organic nanoparticles for ratiometric detection of tyramine in aqueous medium: A novel method to determine food quality. *Food Chemistry, 245*, 1257-1261.

Li, B.-L., Li, Y.-S., & Gao, X.-F. (2019). Fluorescence quenching capillary analysis for determining trace-level nitrite in food based on the citric acid/ethylenediamine nanodots/nitrite reaction. *Food Chemistry, 274*, 162-169.

Li, H., Meininger, C. J., & Wu, G. (2000). Rapid determination of nitrite by reversed-phase high-performance liquid chromatography with fluorescence detection. *Journal of Chromatography B: Biomedical Sciences and Applications, 746*(2), 199-207.

Li, H., Zhao, Y., Chen, Z., & Xu, D. (2017). Silver enhanced ratiometric nanosensor based on two adjustable Fluorescence Resonance Energy Transfer modes for quantitative protein sensing.

Biosensors and Bioelectronics, 87, 428-432.

Lin, T.-W., Dhenadhayalan, N., Lee, H.-L., Lin, Y.-T., Lin, K.-C., & Chang, A. H. H. (2019). Fluorescence turn-on chemosensors based on surface-functionalized MoS2 quantum dots. *Sensors and Actuators B: Chemical, 281*, 659-669.

Liu, H., Yang, G., Abdel-Halim, E. S., & Zhu, J.-J. (2013). Highly selective and ultrasensitive detection of nitrite based on fluorescent gold nanoclusters. *Talanta, 104*, 135-139.

Niedzielski, P., Kurzyca, I., & Siepak, J. (2006). A new tool for inorganic nitrogen speciation study: Simultaneous determination of ammonium ion, nitrite and nitrate by ion chromatography with post-column ammonium derivatization by Nessler reagent and diode-array detection in rain water samples. *Analytica Chimica Acta, 577*(2), 220-224.

Niu, W.-J., Shan, D., Zhu, R.-H., Deng, S.-Y., Cosnier, S., & Zhang, X.-J. (2016). Dumbbell-shaped carbon quantum dots/AuNCs nanohybrid as an efficient ratiometric fluorescent probe for sensing cadmium (II) ions and l-ascorbic acid. *Carbon, 96*, 1034-1042.

Ortiz-Gomez, I., Ortega-Muñoz, M., Salinas-Castillo, A., Álvarez-Bermejo, J. A., Ariza-Avidad, M., de Orbe-Payá, I., Santoyo-Gonzalez, F., & Capitan-Vallvey, L. F. (2016). Tetrazine-based chemistry for nitrite determination in a paper microfluidic device. *Talanta, 160*, 721-728.

Pan, F., Chen, D., Zhuang, X., Wu, X., Luan, F., Zhang, S., Wei, J., Xia, S., & Li, X. (2018). Fabrication of gold nanoparticles/l-cysteine functionalized graphene oxide nanocomposites and application for nitrite detection. *Journal of Alloys and Compounds, 744*, 51-56.

Qi, Z., You, Q., & Chen, Y. (2016). Nucleotide/Tb3+ coordination polymer nanoparticles as luminescent sensor and scavenger for nitrite ion. *Analytica Chimica Acta, 902*, 168-173.

Ruri Kikurahanajiri, And, R. S. M., ‡, & §, S. M. L. (2002). Indirect Measurement of Nitric Oxide Production by Monitoring Nitrate and Nitrite Using Microchip Electrophoresis with Electrochemical Detection. *Analytical Chemistry, 74*(24), 6370.

Santoro, S., Moro, A. J., Portugal, C., Crespo, J. G., Lima, J. C., & Coelhoso, I. M. (2016). Monitoring oxygen permeation through polymeric packaging films using a ratiometric luminescent sensor. *Journal of Food Engineering, 189*, 37-44.

Shen, S.-L., Huang, X.-Q., Zhang, Y.-Y., Zhu, Y., Hou, C., Ge, Y.-Q., & Cao, X.-Q. (2018). Ratiometric fluorescent probe for the detection of HOCl in lysosomes based on FRET strategy. *Sensors and Actuators B: Chemical, 263*, 252-257.

Sun, J., Yang, F., Zhao, D., & Yang, X. (2014). Highly Sensitive Real-Time Assay of Inorganic Pyrophosphatase Activity Based on the Fluorescent Gold Nanoclusters. *Analytical Chemistry, 86*(15), 7883-7889.

Swaminathan, H., & Balasubramanian, K. (2018). Förster resonance energy transfer between MoS2 quantum dots and polyaniline for turn-on bovine serum albumin sensing. *Sensors and Actuators B: Chemical, 264*, 337-343.

Viboonratanasri, D., Pabchanda, S., & Prompinit, P. (2018). Rapid and simple preparation of rhodamine 6G loaded HY zeolite for highly selective nitrite detection. *Applied Surface Science, 440*, 1261-1268.

Wan, Y., Zheng, Y. F., Wan, H. T., Yin, H. Y., & Song, X. C. (2017). A novel electrochemical sensor based on Ag nanoparticles decorated multi-walled carbon nanotubes for applied determination of nitrite. *Food Control, 73*, 1507-1513.

Wang, L., Cao, H.-X., He, Y.-S., Pan, C.-G., Sun, T.-K., Zhang, X.-Y., Wang, C.-Y., & Liang, G.-X. (2019). Facile preparation of amino-carbon dots/gold nanoclusters FRET ratiometric fluorescent probe for

422 sensing of Pb2+/Cu2+. *Sensors and Actuators B: Chemical, 282*, 78-84.
423 Wang, Q., Ma, S., Huang, H., Cao, A., Li, M., & He, L. (2016). Highly sensitive and selective
424 spectrofluorimetric determination of nitrite in food products with a novel fluorogenic probe.
425 *Food Control, 63*, 117-121.
426 Xie, H., Dong, J., Duan, J., Waterhouse, G. I. N., Hou, J., & Ai, S. (2018). Visual and ratiometric
427 fluorescence detection of Hg2+ based on a dual-emission carbon dots-gold nanoclusters
428 nanohybrid. *Sensors and Actuators B: Chemical, 259*, 1082-1089.
429 Xu, X., Qiao, J., Li, N., Qi, L., & Zhang, S. (2015). Fluorescent probe for turn-on sensing of l-cysteine by
430 ensemble of AuNCs and polymer protected AuNPs. *Analytica Chimica Acta, 879*, 97-103.
431 Xu, Y., Niu, X., Zhang, H., Xu, L., Zhao, S., Chen, H., & Chen, X. (2015). Switch-on Fluorescence Sensing of
432 Glutathione in Food Samples Based on a Graphitic Carbon Nitride Quantum Dot (g-CNQD)-
433 Hg2+ Chemosensor. *Journal of agricultural and food chemistry, 63*(6), 1747-1755.
434 Xue, Y., Wang, Z., Ouyang, X., & Qiu, X. (2019). Lignosulfonate: A Convenient Fluorescence Resonance
435 Energy Transfer Platform for the Construction of a Ratiometric Fluorescence pH-Sensing Probe.
436 *Journal of agricultural and food chemistry, 67*(4), 1044-1051.
437 Yang, J., Elim, H. I., Zhang, Q., Lee, J. Y., & Ji, W. (2006). Rational Synthesis, Self-Assembly, and Optical
438 Properties of PbS−Au Heterogeneous Nanostructures via Preferential Deposition. *Journal of*
439 *the American Chemical Society, 128*(36), 11921-11926.
440 Yang, X., Jia, Z., Tan, Z., Xu, H., Luo, N., & Liao, X. (2016). Determination of melamine in infant formulas
441 by fluorescence quenching based on the functionalized Au nanoclusters. *Food Control, 70*, 286-
442 292.
443 Yu, X., Zhang, C.-X., Zhang, L., Xue, Y.-R., Li, H.-W., & Wu, Y. (2018). The construction of a FRET assembly
444 by using gold nanoclusters and carbon dots and their application as a ratiometric probe for
445 cysteine detection. *Sensors and Actuators B: Chemical, 263*, 327-335.
446 Ze, L., Yueqiu, G., Xujun, L., & Yong, Z. (2017). MoS2-modified ZnO quantum dots nanocomposite:
447 Synthesis and ultrafast humidity response. *Applied Surface Science, 399*, 330-336.
448 Zhang, F., Zhu, X., Jiao, Z., Liu, X., & Zhang, H. (2018). Sensitive naked eye detection and quantification
449 assay for nitrite by a fluorescence probe in various water resources. *Spectrochimica Acta Part*
450 *A: Molecular and Biomolecular Spectroscopy, 200*, 275-280.
451 Zheng, X.-J., Liang, R.-P., Li, Z.-J., Zhang, L., & Qiu, J.-D. (2016). One-step, stabilizer-free and green
452 synthesis of Cu nanoclusters as fluorescent probes for sensitive and selective detection of
453 nitrite ions. *Sensors and Actuators B: Chemical, 230*, 314-319.
454
455

Table Captions

Table.1 Comparison with the results for the determination of nitrite by other methods.

Table.2 Recoveries of nitrite in sausage samples.

Figure Captions

Fig.1 The TEM images of prepared MoS_2 QDs (A), AuNCs (B) and MoS_2 QDs-AuNCs composite (C); XRD pattern (D) and FT-IR spectrum (E) of MoS_2 QDs, AuNCs and MoS_2 QDs-AuNCs composite; UV–vis spectrum (F) of MoS_2 QDs and AuNCs.

Fig.2 (A) The fluorescence emission spectrum of MoS_2 QDs (1.0 mL+4.0 mL PBS solution), AuNCs (0.6 mL+4.4 mL PBS solution) and MoS_2 QDs-AuNCs composite (1.0 mL+4.0 mL PBS solution), excitation at 365 nm; (B) the effect of different AuNCs concentration on fluorescence performance of MoS_2 QDs (1.0 mL); (C) the fluorescence and absorption spectrums of MoS_2 QDs and AuNCs, respectively; (D) the fluorescence lifetime of MoS_2 QDs and MoS_2 QDs-AuNCs.

Fig.3 The emission spectrums of MoS_2 QDs (a=1.0 mL, b=1.0 mL+1.0 mL NO_2^- (10 mg/L)), AuNCs (c=0.6 mL, d=0.6 mL+1.0 mL NO_2^- (10 mg/L)) and MoS_2 QDs-AuNCs (e=1.0 mL, f=1.0 mL+1.0 mL NO_2^- (10 mg/L)), excitation at 365 nm.

Fig.4 The schematic diagram for nitrite detection.

Fig.5 The effects of pH (A) and reaction time (B) on the performance of MoS_2 QDs-AuNCs probe.

Fig.6 (A) Fluorescence spectra of the MoS_2 QDs-AuNCs probe in the presence of different concentrations of nitrite (from top to bottom: 0, 0.1, 0.5, 1, 2, 5, 8, 10, 15, 20, 25, 30, 40 and 50 mg/L, respectively. Excitation at 365 nm); the insert: fluorescence color changes of the system at the nitrite concentration of 0 mg/L and 20 mg/L,

479 respectively; (B) the changes of I_{615}/I_{430} value with the nitrite concentration increased
480 from 0-50 mg/L; the insert: the linearity of the system towards the nitrite concentration
481 in the range of 0.5-20 mg/L.
482 **Fig.7** Fluorescence color (A) and 'a' channel grayscale (B) changes with the increase
483 of nitrite concentration (0-25 mg/L), excitation at 365 nm; (C) the linearity of the 'a'
484 value towards different concentrations of nitrite.
485

Table.1 Comparison with the results for the determination of nitrite by other methods.

Method	Linear range	Limit of detection	Reference
Rh6G-HY (fluorometry)	0.04–20.0 mg/L	290 nM	(Viboonratanasri, et al., 2018)
Cu nanoclusters (fluorometry)	0.86 μg/L-345 mg/L	3.6 nM	(Zheng, et al., 2016)
AuNCs (fluorometry)	1.38 μg/L-3.45 mg/L	1.0 nM	(Liu, et al., 2013)
Griess reagent (colorimetry)	15.18 μg/L-3.31 mg/L	20 nM	(Abbas & Mostafa, 2000)
AuNPs/GO-SH (electrochemistry)	0.345-69 mg/L	250 nM	(Pan, et al., 2018)
PyI (fluorometry)	0-0.69 mg/L	100 nM	(Zhang, Zhu, Jiao, Liu, & Zhang, 2018)
MoS_2 QDs-AuNCs system (fluorometry and visualization)	0.5-20 mg/L (fluorometry)	0.67 nM	This work
	1.0-20 mg/L (Visualization)	27.32 nM	

489 **Table.2** Recovery test of nitrite in sausage samples.

Sausage sample	Spiked (mg/L)	Fluorescence method		Visualized analysis	
		Measured (mg/L)	Recovery (%)	Measured (mg/L)	Recovery (%)
1	0.0	0.16	-	0.22	-
2	5.0	5.41	108.2	5.54	110.8
3	10.0	10.37	103.7	10.46	104.6
4	15.0	15.39	102.6	16.03	106.9

490

491

Graphical abstract

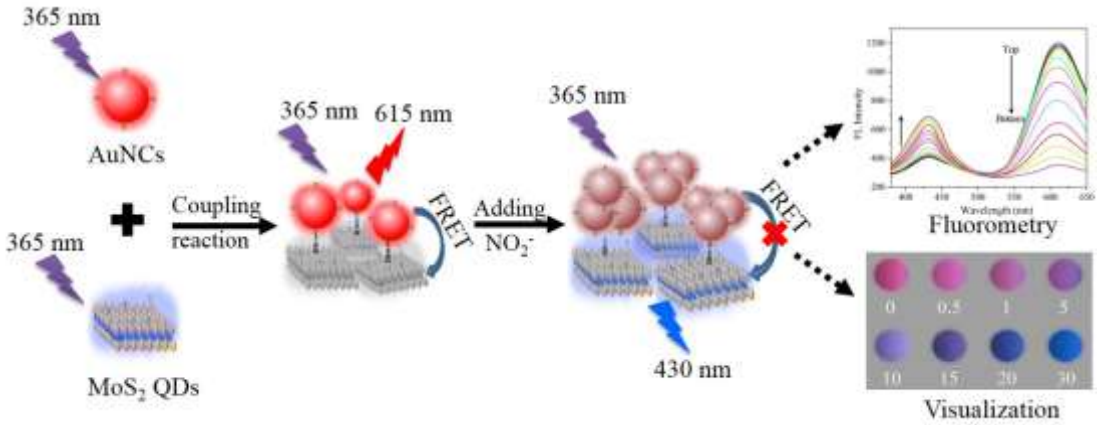

494 **Fig.1**

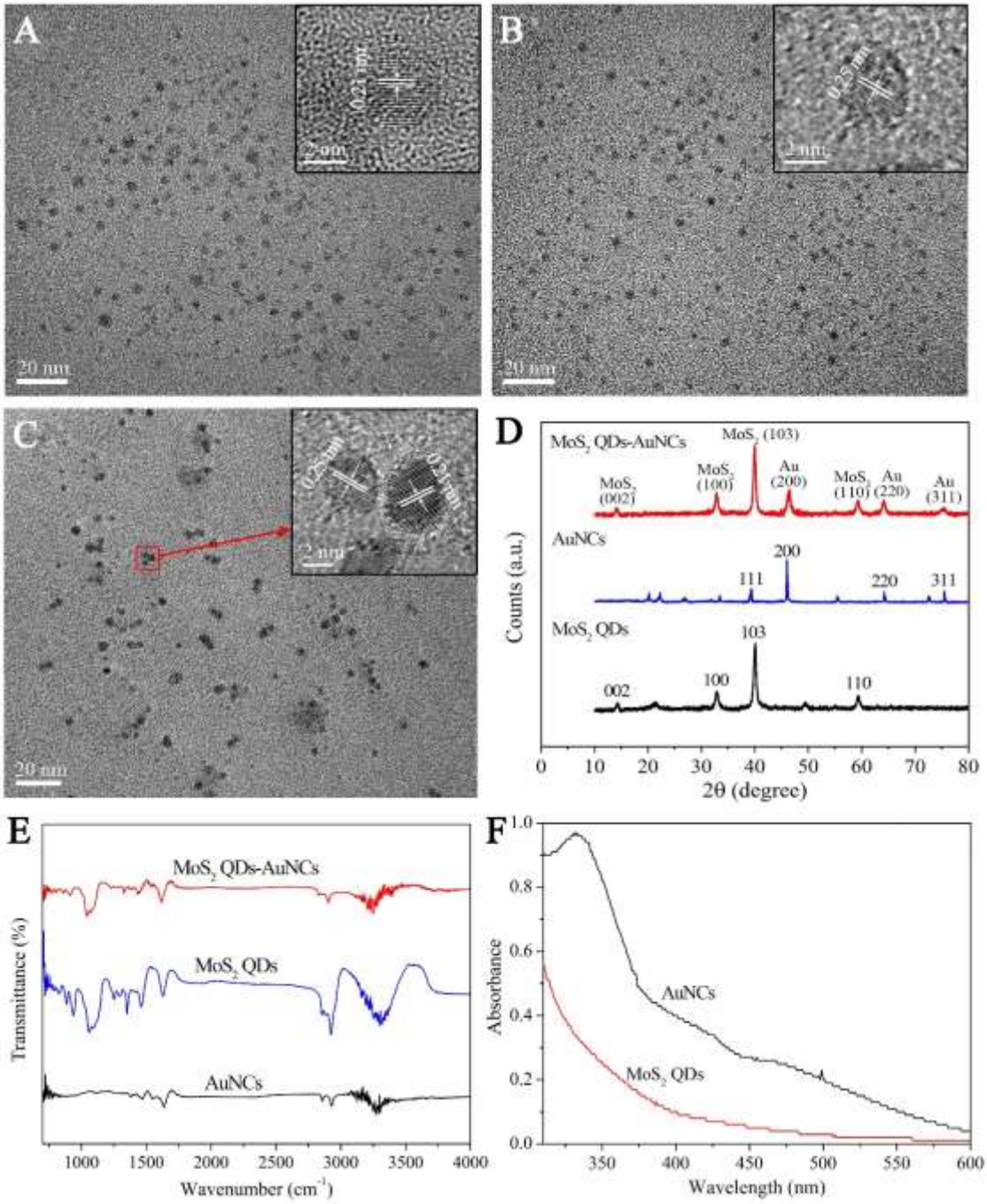

495

496

Fig.2

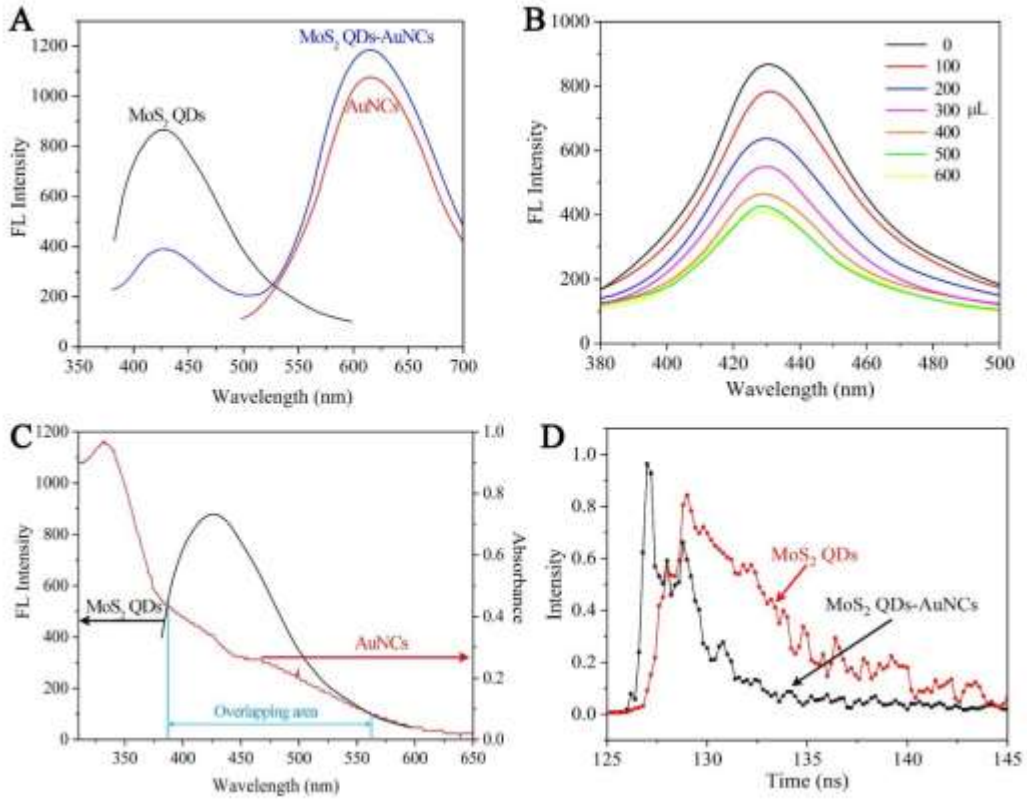
A
MoS2 QDs-AuNCs
MoS2 QDs
AuNCs
FL Intensity
Wavelength (nm)
B
0
100
200
300 μL
400
500
600
FL Intensity
Wavelength (nm)
C
MoS2 QDs
AuNCs
Overlapping area
FL Intensity
Absorbance
Wavelength (nm)
D
MoS2 QDs
MoS2 QDs-AuNCs
Intensity
Time (ns)

501 **Fig.3**

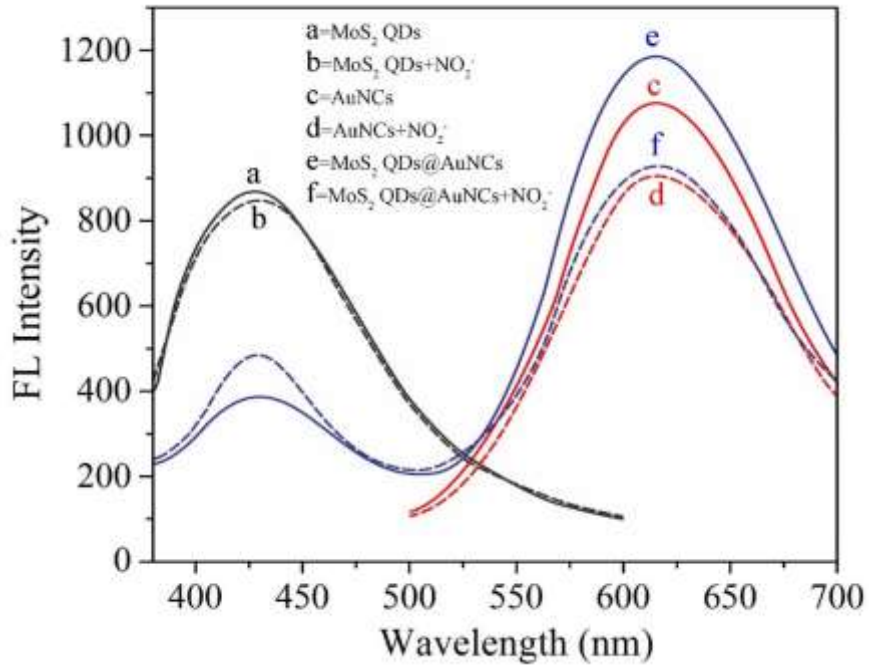

502

503

504

505 **Fig.4**

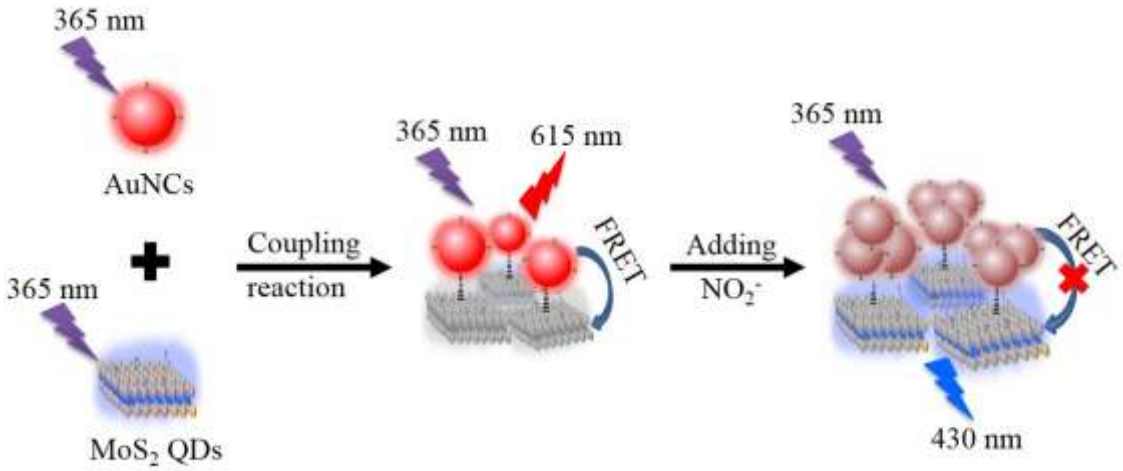

506

507

508

509

510 **Fig.5**

511

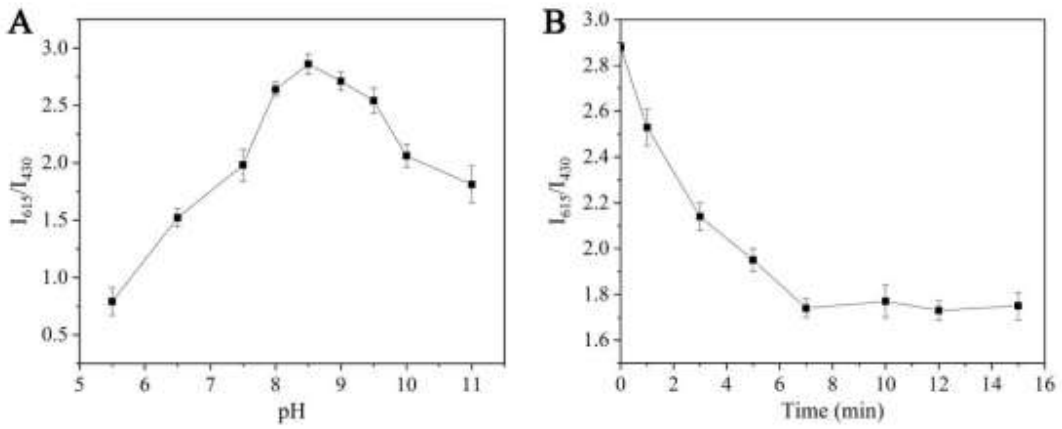

512

513

514 **Fig.6**

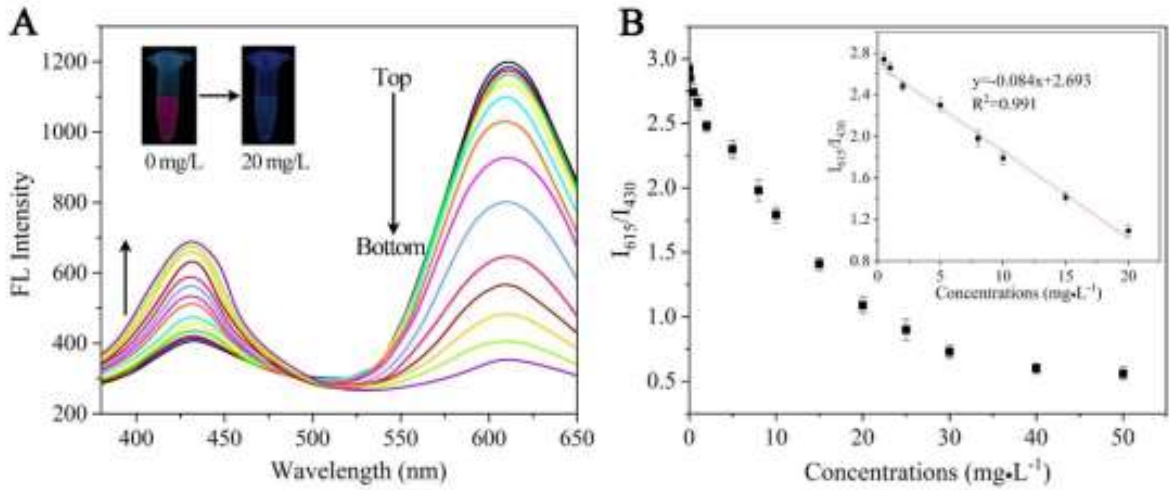

515

516

517

518 **Fig.7**

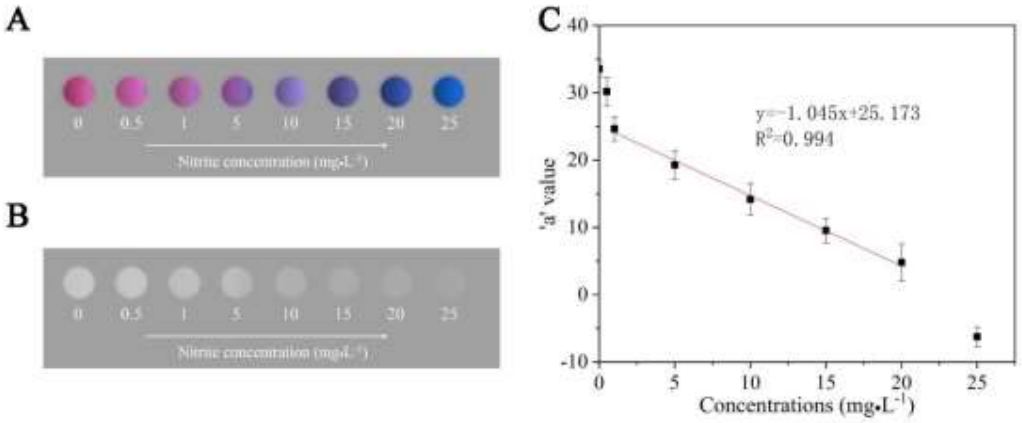
A
0
0.5
1
5
10
15
20
25
Nitrite concentration (mg·L⁻¹)
B
0
0.5
1
5
10
15
20
25
Nitrite concentration (mg·L⁻¹)
C
y=-1.045x+25.173
R²=0.994
'a' value
Concentrations (mg·L⁻¹)

519